frontiers | Frontiers in Energy Research

TYPE Original Research
PUBLISHED 13 March 2024
DOI 10.3389/fenrg.2024.1373851

OPEN ACCESS

EDITED BY
Jiehao Wang,
Chevron, United States

REVIEWED BY
Jianwei Tian,
Technical University of Denmark, Denmark
Jun Liu,
Sichuan University, China

*CORRESPONDENCE
Yongping Wan,
yongpingw19@163.com,
wanhunter@163.com

RECEIVED 20 January 2024
ACCEPTED 28 February 2024
PUBLISHED 13 March 2024

CITATION
Wang X, Zhang Q and Wan Y (2024), A two-phase, multi-component model for efficient CO_2 storage and enhanced gas recovery in low permeability reservoirs.
Front. Energy Res. 12:1373851.
doi: 10.3389/fenrg.2024.1373851

A two-phase, multi-component model for efficient CO_2 storage and enhanced gas recovery in low permeability reservoirs

Xiangzeng Wang, Quan Zhang and Yongping Wan*

Shaanxi Yanchang Petroleum (Group) Co., Ltd., Xi'an, China

Introduction: Carbon dioxide (CO_2) enhanced gas recovery represents a viable strategy for sequestering CO_2 while concurrently augmenting gas production from subsurface reservoirs. Gas reservoirs, as inherent geological formations, are optimal repositories for gaseous compounds, rendering them suitable for CO_2 storage. Nevertheless, the economic viability of pure CO_2 storage necessitates integration with oil and gas recovery mechanisms to facilitate widespread CO_2 utilization.

Method: This study addresses the complexities of CO_2 enhanced gas recovery through a comprehensive approach that combines theoretical model and numerical simulations. A numerical model is developed to simulate three-component diffusion involving CO_2, and methane (CH_4) in a two-phase system comprising gas and water.

Results: The investigation systematically explores the process of enhanced CH_4 extraction and CO_2 injection into the reservoir and examines the influencing factors on extraction. Simulation results reveal a power-law decrease in CH_4 production rate, stabilizing at a constant extraction rate. Enhanced CH_4 extraction benefits from increased porosity, with higher porosity levels leading to greater CH_4 extraction. Permeability augmentation positively influences CH_4 production, although with diminishing returns beyond a certain threshold. The CO_2 injection rate shows a direct proportionality to CH_4 production. However, elevated CO_2 injection rates may increase reservoir pressure, potentially causing cap rock damage and CO_2 gas flushing.

Discussion: This study contributes valuable theoretical insights to the field of CO_2 enhanced gas recovery engineering, shedding light on the intricate dynamics of multi-component fluid transport processes and their implications for sustainable CO_2 utilization.

KEYWORDS

CO_2 geological storage, CO_2-EGR, two-phase flow, multi-component diffusion, low permeability reservoir

1 Introduction

CO_2 is the main greenhouse gas. In order to mitigate and ameliorate the impact of the greenhouse effect on human life, countries around the world are actively taking measures and countermeasures to reduce CO_2 emissions. Among them, CO_2 geological storage has received great attention globally as an effective method to reduce carbon emissions (Bachu, 2000; Weiyang and Chen, 2005; LIU et al., 2005; U. S. Department of Energy and Office of

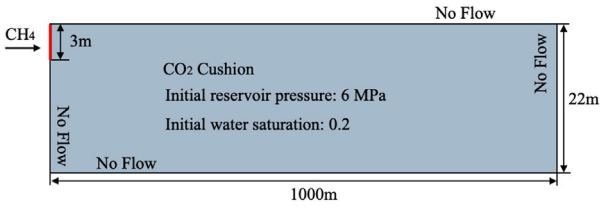

FIGURE 1
Geometric model and boundary conditions of the Oldenburg model.

TABLE 1 Parameter properties of the simulation.

Variable	Numerical	Units
Porosity	0.3	[-]
Permeability	1.0×10^{-13}	[m^2] [m^2]
Temperature	313.15	[K] [Pa · s]
Initial pressure	6.0×10^6	[Pa] [Pa · s]
CH_4 injection rate	1.8375×10^{-2}	[kg/s]
Gas diffusion coefficient	1.0×10^{-6}	[m^2/s]

Fossil Energy and National Energy Technology Laboratory, 2005; Pei et al., 2005; Liu et al., 2005). Common sites for geological storage of CO_2 include deep saline formations, depleted oil and gas reservoirs, unrecoverable reservoirs and oceans (Bonder, 1992; Li and Bai, 2005; XU et al., 2005; Yuchao, 2005; Wu et al., 2008). However, pure CO_2 storage is expensive, so it is necessary to combine the storage with the enhancement of oil and gas recovery to realize the large-scale utilization of CO_2. The gas storage of gas-bearing reservoirs and the closure of the trap have been fully confirmed in the long-term natural gas storage stage and the development stage of natural gas, so it is feasible to realize the buried storage in the gas reservoir.

The mechanism of CO_2 to improve gas recovery mainly has the following four aspects: 1. Increase the reservoir pressure gradient to improve the natural gas seepage rate; 2. The significant density difference between CO_2 and natural gas will lead to gravitational differentiation, so the CO_2 at the bottom of the reservoir has a lifting effect on the natural gas; 3. Under the conditions of temperature and pressure of the reservoir, CO_2 tends to be in a supercritical state, and its viscosity is much higher than that of the natural gas, which produces the ratio of the fluidity that is favorable for the replacement; 4. The CO_2 displaces CH_4 in the reservoir through the competition adsorption effect (Busch et al., 2006; Liang et al., 2010; Katayama, 2023). Enhanced gas recovery using CO_2 not only enables geological storage of CO_2, but also increases CH_4 production (Hamza et al., 2021; Zhang et al., 2023).

The mixing of injected CO_2 and natural gas in the reservoir affects the driving efficiency and leads to the rapid breakthrough of CO_2 in the production wells, resulting in the poor effect of driving the gas to improve recovery, and the CO_2 in the recovered gas further increases the difficulty and cost of the surface treatment process and reduces the comprehensive economic benefits of CO_2-EGR, so it is of great significance to control the CO_2-CH_4 mixing. K. Damen et al. (Damen et al., 2005) analyzed the economics of reservoir geological disposal of CO_2 collected from China using a multi-criteria analysis including technical and socio-economic criteria. Y. Kurniawan et al. (Kurniawan et al., 2006) used numerical simulations to investigate the competitive adsorption of two-component (CH_2-CO_4) gas in crack like pore structures; V. Goetz et al. (Goetz et al., 2006) conducted experimental studies on the adsorption of CO_2 and CH_4 mixed gases on activated carbon and obtained adsorption isotherms for different gases. K. Jessen et al. (Jessen et al., 2008) conducted experimental and simulation studies on CH_4 extraction by gas injection, but the coal samples used were powder synthesized specimens; T. Theodore et al. (Theodore et al., 2004) introduced experimental and simulation studies on CO_2 storage in reservoirs jointly conducted by the University of Southern California and the Australian National University, focusing on the impact of reservoir structure on CO_2 geological disposal.

Indoor experiments on CO_2 and reservoir fluids are often limited by time and space, and the experiments cannot effectively reflect the interaction between CO_2 and reservoir fluids across time and space scales in the CO_2-EGR process. Although numerical simulation can solve the problems of time and space scales, CO_2 and reservoir fluids involve multiphase and multi-component coupling processes. Therefore, numerical models that characterizes the migration of multiple components such as CO_2, CH_4, and reservoir water in reservoirs are needed for numerical simulation analysis of CO_2 enhanced CH_4 recovery.

In this article, we derive the control equation for two-phase, three component flow and establish a numerical model for CO_2 injection and production of CH_4 based on the proposed multiphase multi-component flow theory. We use Partial Differential Equation Module (PDE) of COMSOL for solving the governing equations, studying the migration of CO_2, CH_4

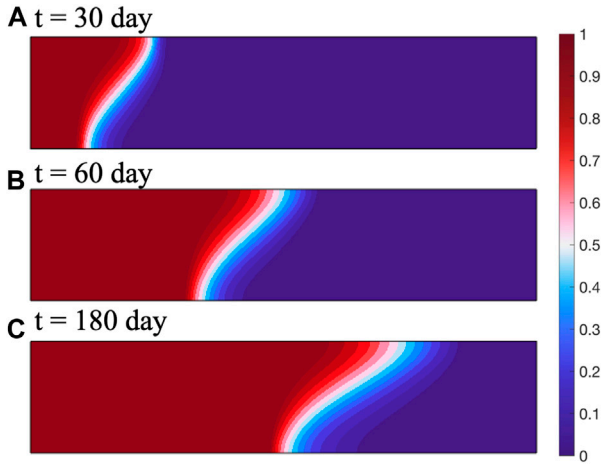

FIGURE 2
Simulation results at **(A)** 30 days, **(B)** 60 days, and **(C)** 180 day.

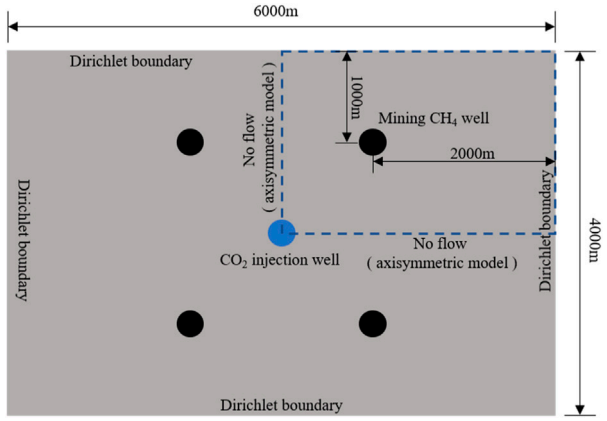

FIGURE 3
Geometry and boundary conditions of the simulation.

and water in the process of CO_2 injection and production in the isotropic reservoir. By changing the permeability, porosity and CO_2 injection rate of the reservoir, we studied the influence of reservoir parameters and injection schemes on the distribution of reservoir stress and the extraction of CH_4.

2 Mathmatical model

2.1 Governing equation of gas-water two-phase flow

Base on the mass conservation of the aquifer fluid, the continuity equation for gas-water two-phase flow is as follows (Martin et al., 2005a; Martin et al., 2005b; Ma et al., 2021; Ma et al., 2023):

$$\frac{\partial m_\alpha}{\partial t} + \nabla \cdot (\rho_\alpha v_\alpha) - q_\alpha = 0, \alpha = w, g \quad (1)$$

where m_α is the fluid mass, q_α is the source (α = w, g represents water and gas, respectively). The fluid velocity is described by Darcy's law:

$$v_\alpha = -\frac{k k_\alpha^r}{\mu_\alpha}(\nabla P_\alpha - \rho_\alpha \boldsymbol{g}) \quad (2)$$

where k represents permeability, and k_α^r is the relative permeability, μ_α is fluid viscosity, P_α is pore pressure, ρ_α is the fluid density, and $\boldsymbol{g}$ is the gravitational acceleration. The mass of each phase can be described as:

$$m_\alpha = S_\alpha \rho_\alpha \phi \quad (3)$$

where S_α is fluid saturation, ρ_α is fluid density, ϕ is porosity.

2.2 Governing equations of gas diffusion

According to Fick's law, the diffusion flux per unit cross-sectional area perpendicular to the diffusion direction per unit time is directly proportional to the concentration gradient at that

TABLE 2 Case parameter settings.

Variable	Numerical	Units
Porosity	0.07	[-]
Permeability	2.0×10^{-15}	[m^2] [m^2]
Entering capillary pressure	1.0×10^5	[Pa] [Pa · s]
Pore distribution index	2	[-]
Residual water saturation	0	[-]
Residual gas saturation	0	[-]
Gas diffusion coefficient	1.0×10^{-5}	[m^3/s] [Pa]

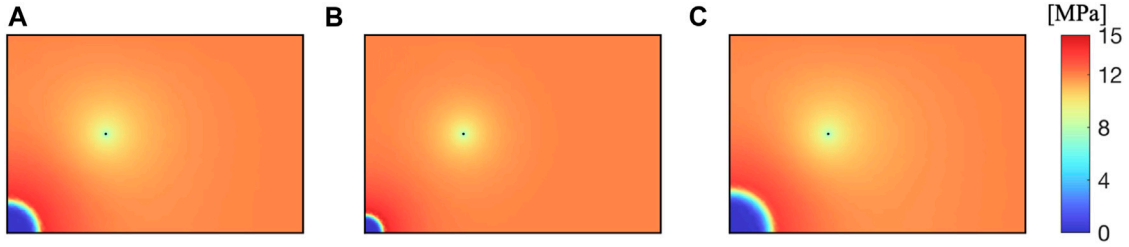

FIGURE 4
(A) 100 days, **(B)** 300 days, and **(C)** 500 days results of CH_4 pressure in reservoirs.

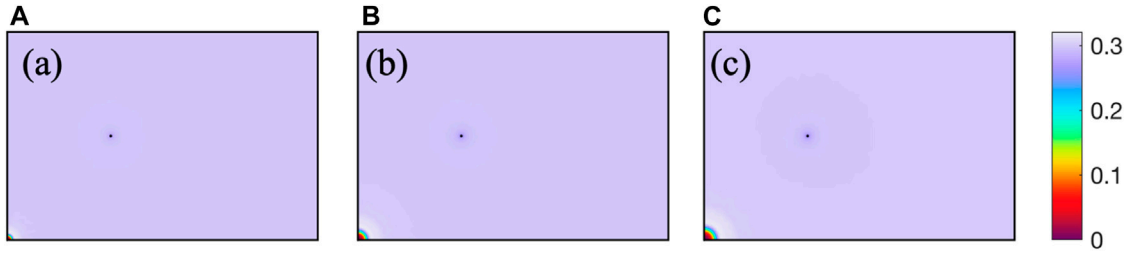

FIGURE 5
(A) 100 days, **(B)** 300 days, and **(C)** 500 days reservoir water saturation results.

cross-section (Nie et al., 2000; Qin et al., 2012; Qin et al., 2013; Li, 2015; Wang, 2015):

$$\left[\frac{\partial}{\partial x}\left(D_{AB}S_g\phi M_A\frac{dC_A}{dx}\right)+\frac{\partial}{\partial y}\left(D_{AB}S_g\phi M_A\frac{dC_A}{dy}\right)+\frac{\partial}{\partial z}\left(D_{AB}S_g\phi M_A\frac{dC_A}{dz}\right)\right]dxdydzdt \quad (4)$$

$$J_A=-D_{AB}\frac{dC_A}{dz} \quad (5)$$

where J_A is the diffusion flux per unit area of component A in the z-direction per unit time; D_{AB} is the diffusion coefficient between components A and B; C_A is the gas concentration of component A, dC_A/dz is the concentration gradient of component A in the z-direction. In the unit, the molecular diffusion flux J_A of component A gas in the gas phase on the left side. Within dt time, the mass of component A gas flowing into the unit through molecular diffusion in the x-direction is:

$$-D_{AB}S_g\phi M_A\frac{dC_A}{dx}dydzdt \quad (6)$$

The mass of component A gas flowing out of the unit through molecular diffusion in the x-direction on the right side of the unit is:

$$\left[\left(-D_{AB}S_g\phi M_A\frac{dC_A}{dx}\right)+\frac{\partial}{\partial x}\left(-D_{AB}S_g\phi M_A\frac{dC_A}{dx}\right)dx\right]dydzdt \quad (7)$$

Within dt time, the mass difference of component A in the unit due to gas diffusion is:

$$-\left[\frac{\partial}{\partial x}\left(v_{gx}M_AC_A\right)+\frac{\partial}{\partial y}\left(v_{gy}M_AC_A\right)+\frac{\partial}{\partial z}\left(v_{gz}M_AC_A\right)\right]dxdydzdt \quad (8)$$

In summary, the gas convection diffusion equation is obtained as follows:

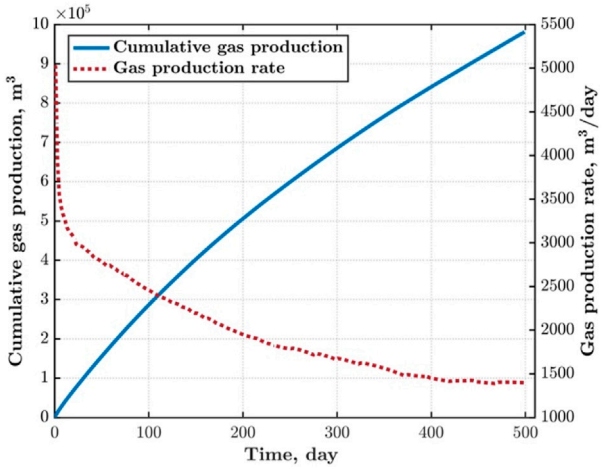

FIGURE 6
CH_4 production volume and daily productivity.

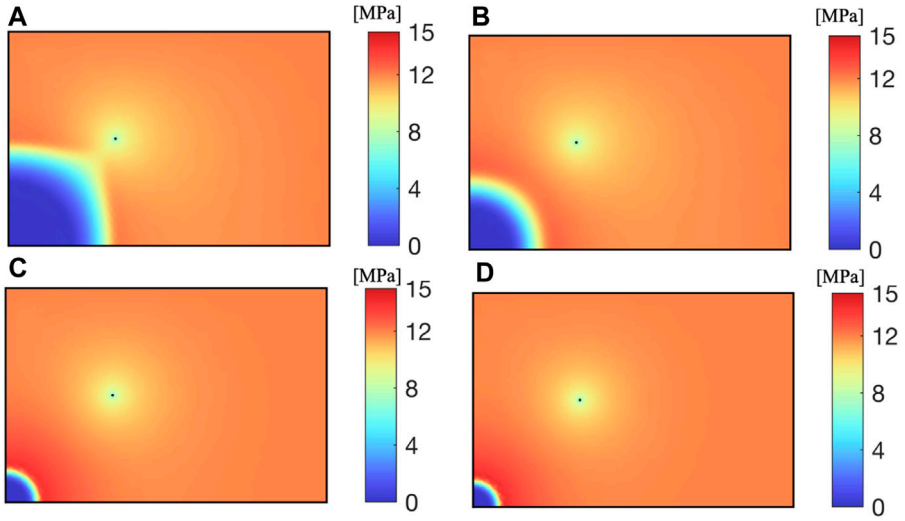

FIGURE 7
CH_4 pressure with different porosities: **(A)**: 0.0175 **(B)**: 0.035 **(C)**: 0.14 **(D)**: 0.21.

$$\frac{\partial\left(\phi M_A C_A S_g\right)}{\partial t} + \nabla\cdot\left(\boldsymbol{v_g} M_A C_A\right) - \nabla\cdot\left(\phi D_{AB} S_g M_A \nabla C_A\right) = 0 \quad (9)$$

2.3 Equation assembly

Substituting Eq. 2 into Eqs 1, 9, the two-phase multi-component seepage model is obtained as follows:

$$\frac{\partial\left(\phi\rho_w S_w\right)}{\partial t} - \nabla\cdot\left(\rho_w \frac{kk_{rw}}{\mu_w}\left(\nabla p_w\right)\right) = 0 \quad (10)$$

$$\frac{\partial\left(\phi M_A C_A S_g\right)}{\partial t} - \nabla\cdot\left(M_A C_A \frac{kk_{rg}}{\mu_g}\left(\nabla p_g\right)\right) - \nabla\cdot\left(\phi D_{AB} S_g M_A \nabla C_A\right) = 0 \quad (11)$$

$$\frac{\partial\left(\phi M_B C_B S_g\right)}{\partial t} - \nabla\cdot\left(M_B C_B \frac{kk_{rg}}{\mu_g}\left(\nabla p_g\right)\right) - \nabla\cdot\left(\phi D_{AB} S_g M_B \nabla C_B\right) = 0 \quad (12)$$

where M_A and M_B are fixed values for the relative molecular weight of the gas, and $\rho = MC$, therefore the equation can be transformed into:

$$\frac{\partial\left(\phi\rho_w S_w\right)}{\partial t} - \nabla\cdot\left(\rho_w \frac{kk_{rw}}{\mu_w}\left(\nabla p_w\right)\right) = 0 \quad (13)$$

$$\frac{\partial\left(\phi\rho_A S_g\right)}{\partial t} - \nabla\cdot\left(\rho_A \frac{kk_{rg}}{\mu_g}\left(\nabla p_g\right)\right) - \nabla\cdot\left(\phi D_{AB} S_g \nabla\rho_A\right) = 0 \quad (14)$$

$$\frac{\partial\left(\phi\rho_A S_g\right)}{\partial t} - \nabla\cdot\left(\rho_B \frac{kk_{rg}}{\mu_g}\left(\nabla p_g\right)\right) - \nabla\cdot\left(\phi D_{AB} S_g \nabla\rho_B\right) = 0 \quad (15)$$

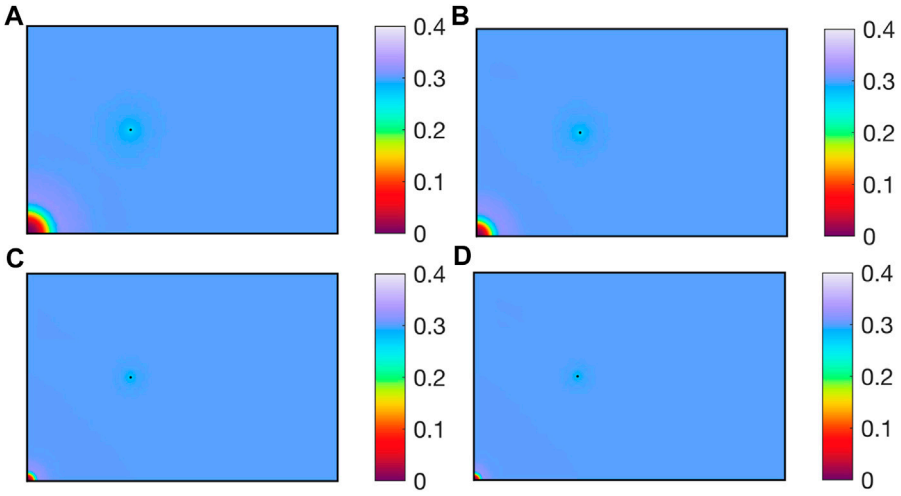

FIGURE 8
Water saturation at different porosities: **(A)**: 0.0175 **(B)**: 0.035 **(C)**: 0.14 **(D)**: 0.21.

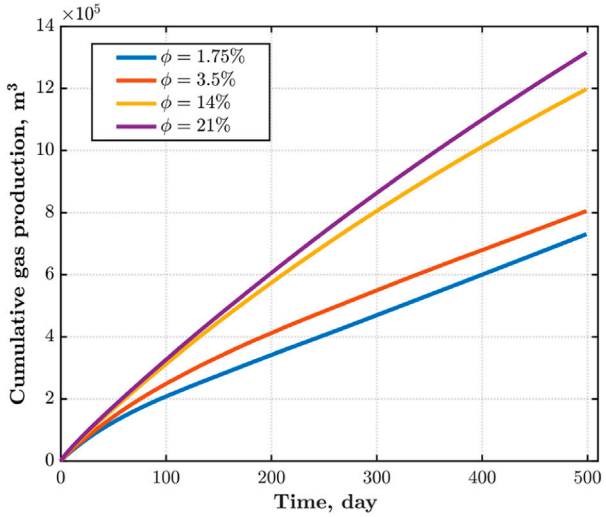

FIGURE 9
CH4 production.

Due to the presence of two gases in the gas phase, the pressures of the two gases are defined as p_A、 p_B:

$$p_g = p_A + p_B \tag{16}$$

Substitute the saturation equation and capillary pressure equation into:

$$\begin{cases} S_w + S_g = 1 \\ p_w = p_g - p_c \end{cases} \tag{17}$$

There are five variables for solving the equation system: S_w、 S_g、 p_w、 p_A and p_B. There are also five equations, which are closed and solvable. The remaining parameters are calculated using the method of calculating physical properties parameters: $\rho_i = \rho_i(p_i); \mu_g = \mu_g(p_g); \mu_w = \mu_w(p_w); k_{rw} = k_{rw}(S_w);\ k_{rw} = k_{rw}(S_w);\ p_c = p_c(S_w)$.

Substitute the equations into and eliminate S_g、 p_w and p_g. We obtain a system of equations for variables S_w、 p_A and p_B:

$$\frac{\partial(\phi\rho_w S_w)}{\partial t} - \nabla\cdot\left(\rho_w\frac{kk_{rw}}{\mu_w}(\nabla(p_A + p_B - p_c))\right) = 0 \tag{18}$$

$$\frac{\partial(\phi\rho_A(1-S_w))}{\partial t} - \nabla\cdot\left(\rho_A\frac{kk_{rg}}{\mu_g}(\nabla(p_A + p_B))\right) - \nabla\cdot(\phi D_{AB}(1-S_w)\nabla\rho_A) = 0 \tag{19}$$

$$\frac{\partial(\phi\rho_B(1-S_w))}{\partial t} - \nabla\cdot\left(\rho_B\frac{kk_{rg}}{\mu_g}(\nabla(p_A + p_B))\right) - \nabla\cdot(\phi D_{AB}(1-S_w)\nabla\rho_B) = 0 \tag{20}$$

According to the Brooks Corey model capillary pressure calculation formula, the capillary pressure is as follows:

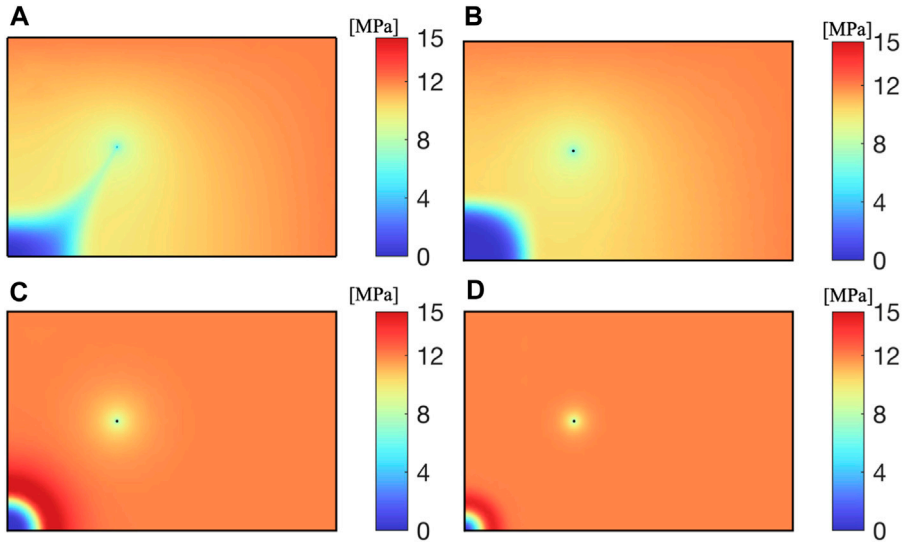

FIGURE 10
CH_4 pressure at different permeabilities **(A)**: $2 \times 10^{-13} m^2$ **(B)**: $2 \times 10^{-14} m^2$ **(C)**: $2 \times 10^{-16} m^2$ **(D)**: $2 \times 10^{-17} m^2$

$$\nabla p_c = \frac{dp_c}{dS_w}\nabla S_w = \frac{P_t(-1/\omega)S_e^{-1/\omega-1}}{1-S_w^r-S_g^r}\nabla S_w \tag{21}$$

$$\frac{\partial p_c}{\partial t} = \frac{dp_c}{dS_w}\frac{\partial S_w}{\partial t} = \frac{P_t(-1/\omega)S_e^{-1/\omega-1}}{1-S_w^r-S_g^r}\frac{\partial S_w}{\partial t} \tag{22}$$

The final control equation is as follows:

$$\left(\phi\rho_w - \phi\rho_w c_w S_w \frac{dp_c}{dS_w}\right)\frac{\partial S_w}{\partial t} + (\phi\rho_w c_w S_w)\frac{\partial p_A}{\partial t} + (\phi\rho_w c_w S_w)\frac{\partial p_B}{\partial t} - \nabla\cdot\left(\rho_w \frac{kk_w^r}{\mu_w}\left(\nabla p_A + \nabla p_B - p_c^{'}\nabla S_w\right)\right) = 0 \tag{23}$$

$$\left(-\phi\rho_A\right)\frac{\partial S_w}{\partial t} + \left(\rho_A(1-S_w) + \phi\rho_A^{'}(1-S_w)\right)\frac{\partial p_A}{\partial t} + \left(\phi\rho_A^{'}(1-S_w)\right)\frac{\partial p_B}{\partial t} - \nabla\cdot\left(\rho_A\frac{kk_g^r}{\mu_g}\left(\nabla p_A + \nabla p_B\right)\right)\nabla p_A + \nabla p_B\Bigg)\rho_A\frac{kk_g^r}{\mu_g} - \nabla\cdot\left(\phi D_{AB}(1-S_w)\rho_A^{'}\nabla p_A\right) = 0 \tag{24}$$

$$\left(-\phi\rho_B\right)\frac{\partial S_w}{\partial t} + \left(\phi\rho_B^{'}(1-S_w)\right)\frac{\partial p_A}{\partial t} + \left(\phi\rho_B^{'}(1-S_w)\right)\frac{\partial p_B}{\partial t} - \nabla\cdot\left(\rho_B\frac{kk_g^r}{\mu_g}\left(\nabla p_A + \nabla p_B\right)\right)\Bigg)\rho_B\frac{kk_g^r}{\mu_g} - \nabla\cdot\left(\phi D_{AB}(1-S_w)\rho_B^{'}\nabla p_B\right) = 0 \tag{25}$$

3 Verification

This section verifies the accuracy of the proposed two-phase multi-component model by comparing the results of Oldenburg's simulation scheme (Oldenburg, 2003). The reservoir model has a vertical depth of 22 m and a horizontal length of 1000 m. The wellhead is located on the left boundary of the reservoir, 3 m away from the upper boundary. The remaining boundaries are no-flow. The reservoir model is shown in Figure 1. The reservoir has a constant temperature of 313.15 K, an initial reservoir pressure of 6 MPa, an initial water saturation of 0.2, a gas phase saturation of 0.8, and a gas phase entirely composed of CO_2. The simulation plan involves injecting CH_4 gas into the injection well at a rate of 1.8375×10^{-2} kg/s for 180 days. The parameter properties of the simulation are listed in Table 1.

The simulation results are shown in Figure 2. As the CH_4 is injected, the CO_2 component is continuously pushed towards the right side of the reservoir, and the diffusion zone gradually increases. The distance between the center of the mixed zone and the wellhead gradually increases, the movement rate gradually decreases. This is consistent with the model results of Oldenburg, indicating the applicability and accuracy of this model in gas diffusion problems.

4 Model setup

We set up a reservoir model with a reservoir plane size of 6000 m × 4000 m. The reservoir is homogeneous and isotropic. The initial water saturation of the reservoir is 0.3, and the rest gas is CH_4. The initial reservoir pressure is 12 MPa, the absolute permeability is $K = 2.0 \times 10^{-15} m^2$, and the porosity is 0.07. An injection well is located at the center of the reservoir to inject CO_2, and extraction wells are set at the four corners of the reservoir. The specific location and boundary conditions are shown in Figure 3. The simulation plan involves injecting CO_2 from the injection well at a rate of 0.25 kg/s for 500 days and analyzing the CH_4 rec overy situation. The specific parameters are listed in Table 2.

5 Simulation results

In this section, we discussed CO_2 enhanced CH_4 recovery based on the two-phase multi-component seepage equation. Due to the

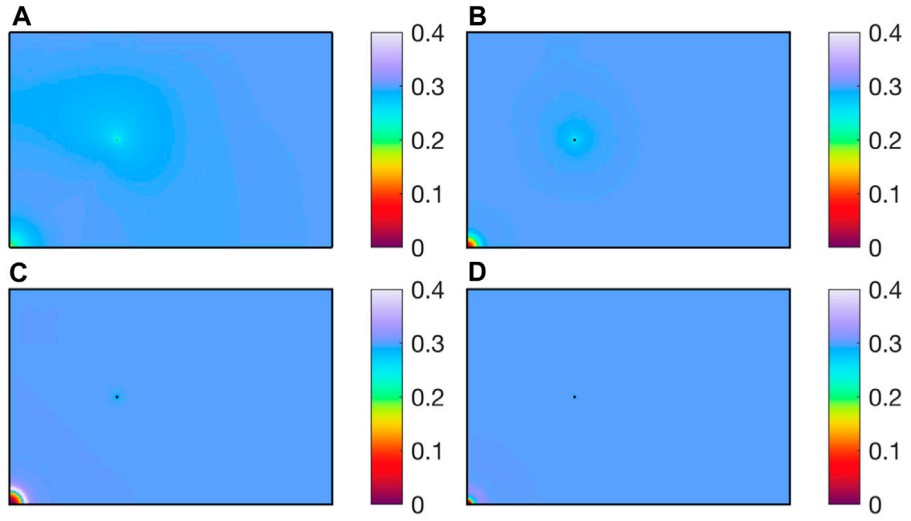

FIGURE 11
Water saturation at different permeabilities: **(A)**: $2 \times 10^{-13} m^2$ **(B)**: $2 \times 10^{-14} m^2$ **(C)**: $2 \times 10^{-16} m^2$ **(D)**: $2 \times 10^{-17} m^2$

geometric distribution of CO_2 injection wells and CH_4 extraction wells being symmetric in the simulation domain, in order to improve computational efficiency, we only analyzed a quarter of the CO_2 displacement CH_4 process.

As shown in Figure 4, after CO_2 is injected into the reservoir, CH_4 inside the reservoir is replaced. The gas pressure of CH_4 near the CO_2 injection well sharply decreases, and as the extraction progresses, CO_2 diffuses towards the vicinity of the extraction well. Near the extraction well, CH_4 pressure decreases uniformly, and CH_4 is extracted through the extraction well.

As shown in Figure 5, after CO_2 is injected into the reservoir, CH_4 and reservoir water are driven away together, forming a CO_2 enrichment zone near the injection well. Near the extraction well, due to the lower well pressure, water and CH_4 are extracted together, decreasing the water saturation.

We study the CH_4 production and daily productivity, as shown in Figure 6, of the extraction wells. Among them, the daily productivity of CH_4 shows a power-law decreasing trend, with CH_4 productivity reaching its maximum in the early stages of extraction; As extraction proceeds, the daily CH_4 production rate decreases due to the decrease in reservoir pressure. In the later stage of extraction, CH_4 productivity reaches equilibrium and remains basically unchanged. The growth rate of production decreases as extraction progresses.

6 Sensitive analysis

6.1 Effect of porosity

In this section, we investigage the distribution of CH_4 pressure, water saturation, and evolution of CH_4 extraction under different reservoir porosities of 0.0175, 0.035, 0.14, and 0.21.

Porosity of reservoir has a significant impact on CH_4 pressure distribution. As shown in the Figure 7, the smaller the porosity of the reservoir, the greater the impact range of CO_2 injection of the same quality. This is because the reduction of pore space results in the same volume of CO_2 occupying a larger reservoir area. When the porosity of the reservoir is 0.0175, the CO_2 injection well and the CH_4 production well are connected, and all the CH_4 in the middle is driven out. When the porosity is greater than 0.14, the influence of porosity on pore pressure decreases.

As shown in Figure 8, the larger the porosity, the larger the pore volume of the same area reservoir, and more CO_2 needs to be injected to expand its influence area; The smaller the porosity, the larger the impact area of the same CO_2 injection amount, and more CH_4 and water from the reservoir pores are driven out by CO_2.

As shown in Figure 9, with the increase of porosity, the CH_4 extraction rate increases; The larger the porosity, the more CH_4 stored near the extraction well. Under the same production well pressure and CO_2 injection rate, the greater the CH_4 production.

6.2 Effect of permeability

In this section, we investigage the distribution of CH_4 pressure, water saturation, and evolution of CH_4 extraction with permeability being with $2 \times 10^{-13} m^2$, $2 \times 10^{-14} m^2$, $2 \times 10^{-16} m^2$ and $2 \times 10^{-17} m^2$.

The permeability of the reservoir determines the migration ability of fluids in the reservoir. As shown in Figure 10, the higher the permeability of the reservoir, the faster CO_2 diffuses from the injection well to the surrounding area at the same time. When the permeability is $2 \times 10^{-13} m^2$, the pressure of the CO_2 injection well and the CH_4 production well interact with each other, and CO_2 flows directly from the injection well to the production well. The lower the permeability, the less CH_4 displaced by CO_2 injection, which is not conducive to CH_4 extraction.

As shown in Figure 11, the influence range of extraction and injection wells is highly correlated with the reservoir permeability. Within the same extraction time, reservoirs with higher permeability can produce more CH_4; Reservoirs with low permeability face greater difficulties in both CO_2 injection and CH_4 extraction, resulting in lower CO_2 recovery efficiency.

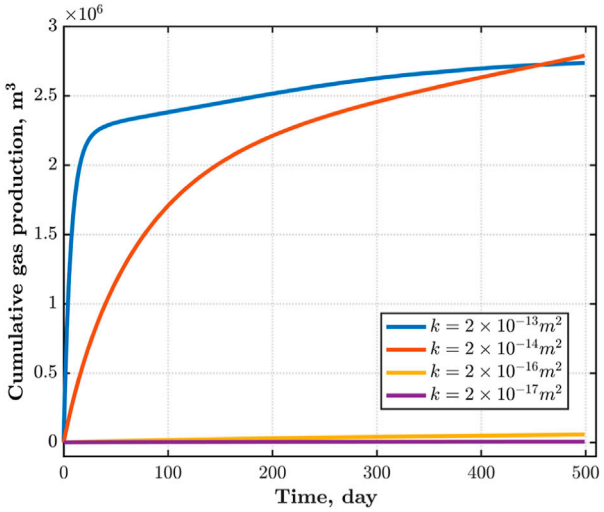

FIGURE 12
CH_4 production under different permeabilities.

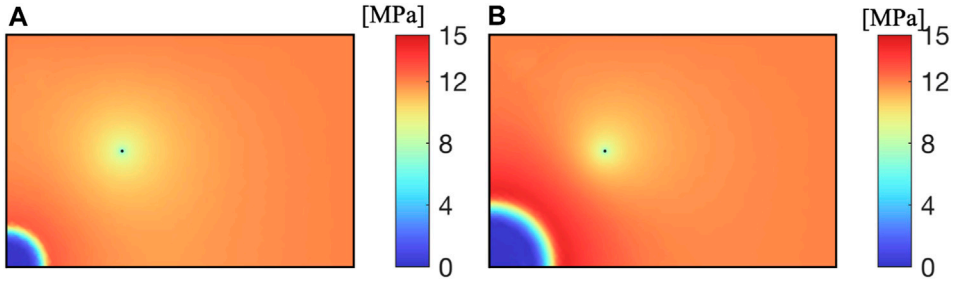

FIGURE 13
CH_4 pressure at different injection rates **(A)**: 0.125 kg/ **(B)**: 0.5 kg/s.

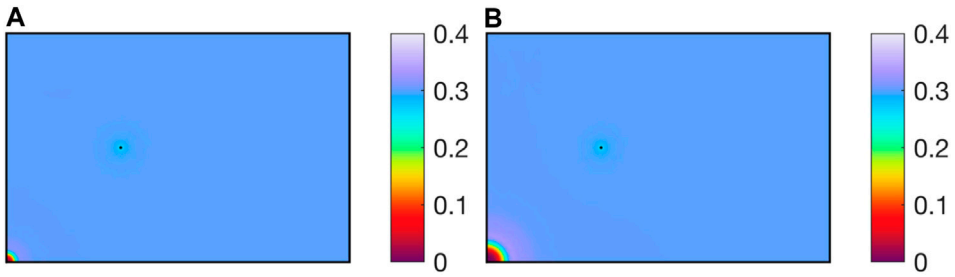

FIGURE 14
Water saturation at different injection rates **(A)**: 0.125 kg/ **(B)**: 0.5 kg/s.

Permeability has a great impact on CH_4 production. As shown in Figure 12, the greater the permeability, the more CH_4 extraction However, blindly increasing the permeability of the reservoir has a saturation value for the increase in CH_4 production. When the permeability of the reservoir increases from $2 \times 10^{-14} m^2$ to $2 \times 10^{-13} m^2$, CH_4 production changes slightly. This may be because the high permeability reservoir causes the injected CO_2 to diffuse to the production well and be extracted. When the permeability reaches a certain level, the reservoir pressure drops too quickly, and the CO_2 injection well and CH_4 production well are connected. After CO_2 breakthrough, The proportion of CH_4 in the production well decreases, making it difficult to extract CH_4.

6.3 Effect of CO_2 injection rate

In this section, we investigage the distribution of CH_4 pressure and water saturation with injection rate being with 0.125 kg/s and 0.5 kg/s.

As shown in Figure 13, the higher the CO_2 injection rate, the greater the reservoir pressure, and the larger the range of CO_2 diffusion. Due to CO_2 injecting water and CH_4 into the pores of the reservoir near the well, the CH_4 pressure near the CO_2 injection well decreases, forming a high-pressure zone at the front of the displacement.

As shown in Figure 14, for water saturation at different injection rates. The higher the CO_2 injection rate, the more water and CH_4 are discharged at the same time, forming a low saturation zone near the injection well. For CH_4 extraction wells, the high pressure brought by high injection rates leads to more CH_4 being extracted, and the high CO_2 injection rate increases CH_4 extraction.

7 Conclusion

The process of CO_2-enhanced CH_4 extraction involves the intricate migration dynamics of gas and water phases, incorporating multiple components within the reservoir. Leveraging the derived two-phase flow and multi-component diffusion model, we present a comprehensive numerical model to elucidate the intricate phenomena associated with the multi-component seepage of CO_2-EGS. This model considers both the water phase and the gas phase, encompassing two distinct components: CO_2 and CH_4. The main conclusions are derived as follows.

1) With the injection of CO_2, both water and CH_4 within the reservoir pores are displaced. The CH_4 productivity exhibits a power-law decline, ultimately stabilizing at a constant extraction rate, with a progressively diminishing gradient of productivity increase. In the initial extraction stages, the CH_4 production rate attains its peak, declining subsequently due to the diminishing reservoir pressure. In the latter stage of extraction, CH_4 productivity reaches an equilibrium state, demonstrating sustained constancy.
2) Higher porosity levels result in augmented CH_4 reserves proximate to extraction wells. However, heightened porosity diminishes the influence of CO_2 on CH_4 recovery, as it reduces the area affected by the reservoir pressure of CO_2. Conversely, lower porosity levels extend the influence of a given CO_2 injection volume over a larger reservoir range, driving out CH_4 and water over an expansive area.
3) Elevated reservoir permeability accelerates CO_2 diffusion from injection wells to the surrounding region. While increased permeability enhances CH_4 production, an indiscriminate escalation of permeability reaches a saturation point for CH_4 production augmentation. Excessive permeability poses the risk of connecting CO_2 injection wells with CH_4 extraction wells, impeding CH_4 extraction upon CO_2 breakthrough.
4) The CO_2 injection rate directly influences the affected area within the reservoir. A higher injection rate results in increased reservoir pressure, leading to greater CH_4 extraction and improved production. Nonetheless, an excessively high CO_2 injection rate induces heightened reservoir pressure, potentially causing cap rock damage and consequent CO_2 release.

Data availability statement

The original contributions presented in the study are included in the article/Supplementary material, further inquiries can be directed to the corresponding author.

Author contributions

XW: Conceptualization, Methodology, Project administration, Visualization, Writing–original draft. QZ: Formal Analysis, Methodology, Visualization, Writing–original draft. YW: Investigation, Methodology, Writing–review and editing.

Funding

The author(s) declare that no financial support was received for the research, authorship, and/or publication of this article.

Acknowledgments

A special acknowledgment goes to the reviewers for their invaluable feedback.

Conflict of interest

Authors XW, QZ, and YW were employed by Shaanxi Yanchang Petroleum (Group) Co., Ltd.

Publisher's note

References

Bachu, S. (2000). Sequestration of CO2 in geological media: criteria and approach for site selection in response to climate change. *Energy Convers. Manag.* 41 (9), 953–970. doi:10.1016/s0196-8904(99)00149-1

Bonder, L. (1992). Applications of carbon dioxide in enhanced oil recovery. *Energy Convers. Manag.* 33 (5), 579–586. doi:10.1016/0196-8904(92)90059-6

Busch, A., Gensterblum, Y., Krooss, B. M., and Siemons, N. (2006). Investigation of high-pressure selective adsorption/desorption behaviour of CO_2 and CH_4 on coals: an experimental study. *Int. J. Coal Geol.* 66 (1-2), 53–68. doi:10.1016/j.coal.2005.07.003

Damen, K., Faaij, A., Van, F., Gale, J., and Lysen, E. (2005). Identification of early opportunity for CO_2 sequestration-worldwide screening for CO_2-EOR and CO_2-ECBM projects. *Energy* 30 (10), 1931–1952. doi:10.1016/j.energy.2004.10.002

Goetz, V., Pupier, O., and Guillot, A. (2006). Carbon dioxide-methane mixture adsorption on activated carbon. *Adsorption* 12 (1), 55–63. doi:10.1007/s10450-006-0138-z

Hamza, A., Hussein, I. A., Al-Marri, M. J., Mahmoud, M., Shawabkeh, R., and Aparicio, S. (2021). CO_2 enhanced gas recovery and sequestration in depleted gas reservoirs: a review. *J. Petroleum Sci. Eng.* 196, 107685–685. doi:10.1016/j.petrol.2020.107685

Jessen, K., Tang, G., and Kovscek, A. (2008). Laboratory and simulation investigation of enhanced coalbed methane recovery by gas injection. *Transp. Porous Media* 73 (2), 141–159. doi:10.1007/s11242-007-9165-9

Katayama, Y. (2023). "Study of coalbed methane in Japan," in *Proceedings of united nations international conference on coalbed methane development and utilization* (Beijin), 238–243.

Kurniawan, Y., Bhatia, S., and Rudolph, V. (2006). Simulation of binary mixture adsorption of methane and CO2 at supercritical conditions in carbons. *AIChE J.* 52 (3), 957–967. doi:10.1002/aic.10687

Li, J. (2015). Mathematical simulation of effect of different coal particle shapes on gas desorption diffusion Law. *Saf. Coal Mines* 46 (1), 1–4.

Liang, W., Wu, D., and Zhao, Y. (2010). Experimental study of coal beds methane replacement by carbon dioxide. *Chin. J. Rock Mech. Eng.* 29 (4), 665–673.

Liu, Q., Wang, Y., Wang, M., et al. (2005a). Trends of greenhouse gases in recent 10 years in Beijing. *Chin. J. Atmos. Sci.* 29 (2), 267–271.

Liu, Y., Li, X., and Bai, B. (2005b). Preliminary estimation of CO_2 storage capacity of coalbeds in China. *Chin. J. Rock Mech. Eng.* 24 (16), 2947–2952.

Li, X., and Bai, B. (2005). Preliminary estimation of CO_2 storage capacity of coalbeds in China. *Chin. J. Rock Mech. Eng.* 24 (16), 2947–2952.

Ma, T., Jiang, L., Shen, W., Cao, W., Guo, C., and Nick, H. M. (2023). Fully coupled hydro-mechanical modeling of two-phase flow in deformable fractured porous media with discontinuous and continuous Galerkin method. *Comput. Geotechnics* 164, 105823. doi:10.1016/j.compgeo.2023.105823

Ma, T., Zhang, K., Shen, W., Guo, C., and Xu, H. (2021). Discontinuous and continuous Galerkin methods for compressible single-phase and two-phase flow in fractured porous media. *Adv. Water Resour.* 156, 104039. doi:10.1016/j.advwatres.2021.104039

Martin, V., Jaffr´e, J., and Roberts, J. E. (2005a). Modeling fractures and barriers as interfaces for flow in porous media. *SIAM J. Sci. Comput.* 26, 1667–1691. doi:10.1137/s1064827503429363

Martin, V., Jaffr´e, J., and Roberts, J. E. (2005b). Modeling fractures and barriers as interfaces for flow in porous media. *SIAM J. Sci. Comput.* 26, 1667–1691. doi:10.1137/s1064827503429363

Nie, B., He, X., and Wang, E. (2000). Mechanism and modes of gas diffusion in coal seams. *China Saf. Sci. J.* 10 (6), 24–28.

Oldenburg, C. M. (2003). Carbon dioxide as cushion gas for natural gas storage. *Energy fuels.* 17, 240–246. doi:10.1021/ef020162b

Pei, K., Sun, S., and Huang, L. (2005). Global warming and carbon dioxide mitigation. *Energy Conserv. Technol.* 23 (3), 239–243.

Qin, Y., Wang, C., Wang, J., et al. (2012). Mathematical model of gas emission in coal particles and the numerical solution. *J. China Coal Soc.* 37 (9), 1466–1471.

Qin, Y., Yongjiang, H., Wang, Y., et al. (2013). Numerical solution of gas emission in coal particle based on two kinds of mathematical model. *J. China Univ. Min. Technol.* 42 (6), 923–928.

Theodore, T., Hiren, P., Fayyaz, N., Racherla, D., Knackstedt, M. A., and Sahimi, M. (2004). Overview of laboratory and modeling studies of carbon dioxide sequestration in coal beds. *Industrial Eng. Chem. Res.* 43 (12), 2887–2901. doi:10.1021/ie0306675

U S Department of Energy, Office of Fossil Energy and National Energy Technology Laboratory (2005). *Carbon sequestration, technology roadmap and program plan*. [S. l.]: U. S. Department of Energy Office of Fossil Energy and National Energy Technology Laboratory.

Wang, J. (2015). Numerical simulation research of gas emission in coal particles based on Darcy' s law. *J. Henan Polytech. Univ. Nat. Sci.* 34 (4), 459–462. 531.

Weiyang, A. I. N., and Chen, J. (2005). Capture and separation of greenhouse gases CO_2—the challenge and opportunity for separation technology. *Chem. Industry Eng. Prog.* 24 (1), 1–4.

Wu, D., Hao, S., and Liang, W. (2008). Development of coal bed methane displacement with carbon dioxide [J]. *Shanxi Coal* 28 (3), 10–14. doi:10.3969/j.issn.1672-5050.2008.03.005

Xu, J., Zhang, J., Pan, X., et al. (2005). Current status of carbon dioxide storage technologies. *Coal Convers.* 28 (3), 80–85.

Yuchao, J. (2005). Ocean disposal of carbon dioxide. *Mar. Sci. Bull.* 24 (2), 72–78.

Zhang, L., Cheng, C., Wen, S., et al. (2023). Thoughts on the development of CO_2-EGR under the background of carbon peak and carbon neutrality. *Nat. Gas. Ind.* 43 (1), 13–22.